Neuro-Learning Based Fault-Tolerant Control of a 2-DOF Helicopter System With Sensor Fault and Unknown Dead Zone

Yan Weng, Zhijia Zhao, *Senior Member, IEEE*, Di Zhang, Zhijie Liu, *Member, IEEE*, and Keum-Shik Hong, *Life Fellow, IEEE*

***Abstract*—Most existing control methods for nonlinear systems rely on adaptive parameters or assume full-state measurability, with limited attention paid to scenarios involving unmeasurable system states. To overcome these shortcomings, this study proposes a neuro-learning based fault-tolerant control strategy for a nonlinear two-degrees-of-freedom (2-DOF) helicopter system with sensor gain faults and an unknown dead zone. First, to address the inaccuracy of state measurements caused by sensor gain faults, a state observer is designed to reconstruct the system states, and adaptive parameters are introduced to estimate the fault in real time, providing compensation information for the controller design. A radial basis function neural network (RBFNN) is employed to address the uncertainties in the nonlinear helicopter system. In addition, the RBFNN, adaptive parameters, and bounded estimation are combined to compensate for the effects of the unknown dead zone. The stability and convergence of the closed-loop system are analyzed using the direct Lyapunov method. In simulations, the observer accurately estimates the actual system states before sensor faults occur, and it responds rapidly and reestablishes accurate state estimation when a fault is introduced. In an experimental validation using a Quanser 2-DOF helicopter platform, the proposed control method provides improved tracking performance and enhanced robustness.**

***Index Terms*—Neural network, sensor fault, two-degrees-of-freedom (2-DOF) helicopter, unknown dead zone.**

I. Introduction

RECENTLY, multirotor uncrewed aerial vehicles (UAVs) have attracted significant interest owing to their strong maneuverability and ability to hover steadily [1], [2], [3]. These features make them highly suitable for complex tasks, such as aerial reconnaissance and disaster rescue [4]. However, a UAV system is inherently a strongly coupled multiple-input multiple-output (MIMO) nonlinear system, characterized by complex dynamics and significant modeling uncertainties. These factors pose major challenges in maintaining system stability and robustness. Therefore, the development of effective control strategies capable of compensating for system nonlinearity is crucial for enhancing the autonomous control performance of unmanned helicopters [5].

The two-degrees-of-freedom (2-DOF) helicopter has the following core challenges: strongly coupled pitch-yaw dynamics, unknown parameters with slow drift, time-varying disturbances, and nonideal perception and actuation systems. Consequently, many researchers utilize the 2-DOF helicopter as a compact, reproducible, real-flight system model to explore solutions for achieving high-precision tracking under such constraints [6], [7], [8]. To address these challenges, various control strategies have been developed to achieve stable control of helicopter systems [9], [10]. However, these studies either linearized the inherently nonlinear helicopter systems or considered model uncertainties within a nonlinear framework, without accounting for the potential input and output constraints.

Unknown dead zone is a typical nonlinear input constraint commonly found in various practical systems, which may degrade the control performance and even lead to system instability [11], [12], [13]. Various compensation strategies have been

Received 16 August 2025; revised 21 October 2025 and 1 December 2025; accepted 2 January 2026. This work was supported in part by the National Natural Science Foundation of China under Grant 62273112, Grant 62473039, Grant 62433011, Grant 62403154, Grant 62573144, and Grant 62522305; in part by Guangdong Basic and Applied Basic Research Foundation under Grant 2025A1515010885, Grant 2023A1515110073, Grant 2024B1515120013, Grant 2023 B1515120018, and Grant 2023B1515120019; in part by the Science and Technology Planning Project of Guangzhou, China under Grant 2025A03J3135 and Grant 2025A04J5629; in part by the Joint Fund of Ministry of Education for Equipment Pre-Research under Grant 8091B03032303; and in part by Beijing Nova Program under Grant 20240484561. *(Corresponding author: Zhijia Zhao.)*

Yan Weng is with the School of Mathematics and Information Science, Guangzhou University, Guangzhou 510006, China (e-mail: 2112207025@e.gzhu.edu.cn).

Zhijia Zhao is with the School of Mechanical and Electrical Engineering and Guangdong Key Laboratory of Low-altitude Intelligent Unmanned Systems Technology for General Universities, Guangzhou University, Guangzhou 510006, China (e-mail: zhaozj@gzhu.edu.cn).

Di Zhang is with the School of Mechanical and Electrical Engineering, Guangzhou University, Guangzhou 510006, China (e-mail: 2112307044@e.gzhu.edu.cn).

Zhijie Liu is with the School of Intelligence Science and Technology, University of Science and Technology Beijing, Beijing 100083, China (e-mail: liuzhijie@ustb.edu.cn).

Keum-Shik Hong is with the Institute for Future, School of Automation, Qingdao University, Qingdao 266071, China, and also with the School of Mechanical Engineering, Pusan National University, Busan 46241, South Korea (e-mail: kshong@pusan.ac.kr).

Digital Object Identifier 10.1109/TIE.2026.3654623

developed to mitigate these effects. The dead-zone problem has been addressed using bounded estimation, smooth functions, and adaptive parameter techniques [14]. The effect on system stability has been effectively eliminated using dead-zone inverse modeling, adaptive control strategies, Lyapunov methods, and parameter estimation [15]. Inverse compensation and adaptive parameter mechanisms have been adopted for error correction [16]. Although significant progress has been made, most existing methods rely on adaptive parameters or assume full-state measurability, with limited attention paid to scenarios involving unmeasurable system states.

Because of its strong nonlinear approximation capability, the radial basis function neural network (RBFNN) has been widely adopted as a key technique for handling bounded uncertainties in nonlinear control systems [17], [18], [19]. Representative studies include the design of a neural network controller in which an RBFNN is employed to manage uncertainties in helicopter systems [20]. A neural network-based adaptive control scheme under an event-triggered mechanism has been developed in which the neural networks approximate unknown nonlinear components and time-varying control gains, thereby enhancing the overall control performance [21]. An adaptive control scheme combining an RBFNN with a disturbance observer has been developed to address the system uncertainties and external disturbances [22]. Similarly, although significant achievements have been made using neural networks to address bounded uncertainties in control systems, these designs generally assume that the state variables are fully known and accurately measured. It should be noted that in certain situations, the system states may be unknown, or discrepancies may exist between the measured and actual states, especially when sensor faults occur, and the measurements fail to reflect the true system behavior. Therefore, to overcome this limitation, further research is required to explore how neural networks can be applied to approximate bounded uncertainties when the system states are not fully available.

In practice, system instability and degraded tracking performance are often encountered owing to actuator or sensor faults, which pose a significant threat to the safety of unmanned systems [23], [24], [25], [26]. Therefore, it is essential to employ an effective technique to reconstruct system states and ensure that the estimated values closely approximate the actual states [27], [28], [29], [30]. Active fault-tolerant control (AFTC) has received considerable attention from researchers because it significantly improves the reliability and safety of fault-affected systems. A sensor fault diagnosis and fault-tolerant control method based on a learning observer has been developed and applied to a robotic arm system subjected to disturbances [31]. In [32], the authors proposed a fault-tolerant control scheme for linear parameter-varying systems, where the estimated fault magnitudes were used to adjust the controller and observer gains, enabling effective fault compensation and preserving system robustness. An AFTC strategy combining interval type-2 fuzzy-logic and sliding-mode control has been introduced, in which a nonlinear adaptive observer is employed to estimate and compensate for sensor and actuator faults in a three-degrees-of-freedom helicopter system in real time [33]. Moreover, Bounemeur et al. developed a series of fuzzy adaptive fault-tolerant control methods that efficiently compensate for deviations caused by actuator and sensor failures in quadrotor systems, thereby significantly enhancing the disturbance rejection capability of the system [34], [35]. Although sensor fault research has advanced considerably, prior efforts seldom evaluated algorithmic performance in real systems. In particular, the coupled effects of unknown input dead zones and sensor-gain faults on helicopter platforms have not been sufficiently investigated. This gap motivates the present study.

The aim of this study is to investigate an AFTC strategy to achieve trajectory tracking control for a 2-DOF helicopter system with sensor faults and unknown dead zones. The primary contributions of this study are summarized as follows.

1) When sensor gain faults occur in the system, the state measurements become inaccurate. To address this issue, the proposed solution implements a state observer, which corrects the system state in the presence of sensor gain faults. Adaptive parameters are introduced to estimate the faults in real time, providing the basis for fault compensation in the controller. Compared with the observer proposed in [36], the observer designed in this study estimates sensor faults more accurately, thereby enhancing system robustness.
2) Prior studies [34] and [35] proposed effective fault-tolerant controllers and achieved good results on MIMO nonlinear platforms, including quadrotors. However, several limitations remain. First, fuzzy-logic systems rely on rule bases and membership functions. When adapted online, the number of rules can grow rapidly, which raises computation cost. Second, input constraints are not handled in a systematic way; therefore, real-time performance is difficult to maintain under high sampling rates and strong coupling. Moreover, some works did not include hardware tests; thus, performance and convergence under constrained and disturbed conditions were not fully assessed. By contrast, the proposed approach combines an RBFNN with an observer-based fault reconstruction and directly compensates the input dead zone.
3) Although significant progress has been made in addressing unknown dead-zone problems, most existing approaches either design adaptive compensation schemes based on smooth functions or utilize neural networks to estimate the nonlinear effects caused by dead zones. However, adaptive compensation methods are typically tailored for symmetric dead zones and often perform poorly when handling asymmetric nonlinearities. Moreover, neural networks generally require measurable system states as inputs, which may become unavailable in the presence of sensor failures or other physical faults. Therefore, it is imperative to develop compensation strategies that can effectively handle input dead zones.

The remainder of this article is organized as follows. Section II presents the 2-DOF helicopter model, sensor fault description, and useful preliminaries. Section III details the observer-based fault reconstruction and RBFNN adaptive controller with smooth regularization. Section IV presents

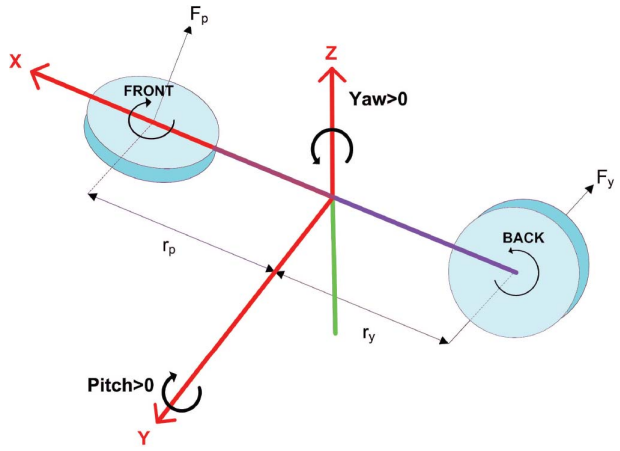

Fig. 1. Model of a 2-DOF helicopter [37].

simulation studies that were performed to evaluate tracking and robustness. Section V discusses the hardware experiments and results. Finally, Section VI concludes the article.

II. Problem and Preliminary Formulation

A. Problem Formulation

The 2-DOF helicopter model is shown in Fig. 1. The helicopter motion is regulated by the front and back dc motors, which produce thrust forces F_p and F_y, respectively, and are responsible for controlling the pitch angle θ and yaw angle ψ.

Using the Euler-Lagrange equations, the dynamics of the 2-DOF helicopter system are formulated as follows:

$$(J_p + ml^2)\ddot{\theta} = K_{pp}V_{pp} + K_{py}V_{yy} - mGl\cos(\theta) - D_{pp}\dot{\theta} - ml^2\dot{\psi}^2\cos(\theta)\sin(\theta) \quad (1)$$

$$(J_y + ml^2\cos^2(\theta))\ddot{\psi} = K_{yp}V_{pp} + K_{yy}V_{yy} - D_{yy}\dot{\psi} + 2ml^2\dot{\theta}\dot{\psi}\cos(\theta)\sin(\theta) \quad (2)$$

where θ and ψ represent the pitch and yaw angles, respectively; m is the mass of the helicopter; l represents the distance between the helicopter's center of mass and the fixed reference frame; D_{yy} and D_{pp} denote the viscous friction coefficients for pitch and yaw motions, respectively; G is the gravitational constant; J_y and J_p represent the moments of inertia of the rotating beam about the yaw and pitch axes, respectively; and K_{pp}, K_{py}, K_{yp}, and K_{yy} denote the thrust torque constants.

We set the state variable as $x = [x_1, x_2]^T$, where $x_1 = [\theta, \psi]^T$ and $x_2 = [\dot{\theta}, \dot{\psi}]^T$, and the input variables $u = [V_{pp}, V_{yy}]^T$. Therefore, (1) and (2) can be transformed into state-space equations

$$\dot{x}_1 = x_2 \quad (3)$$

$$\dot{x}_2 = A(x) + B(x)u + \Delta A(x) \quad (4)$$

$$y = x_1 \quad (5)$$

where $\Delta A(x)$ denotes the uncertainty of the system, and the expressions for the functions $A(x)$ and $B(x)$ are

$$A(x) = \begin{bmatrix} \frac{a_{11}}{a_{12}} \\ \frac{a_{21}}{a_{22}} \end{bmatrix}, \quad B(x) = \begin{bmatrix} \frac{K_{pp}}{a_{12}} & \frac{K_{py}}{a_{12}} \\ \frac{K_{yp}}{a_{22}} & \frac{K_{yy}}{a_{22}} \end{bmatrix} \quad (6)$$

where

$$\begin{aligned} a_{11} &= -mGl\cos(\theta) - D_{pp}\dot{\theta} - ml^2\dot{\psi}^2\sin(\theta)\cos(\theta) \\ a_{12} &= J_p + ml^2 \\ a_{21} &= -D_{yy}\dot{\psi} + 2ml^2\dot{\psi}\dot{\theta}\sin(\theta)\cos(\theta) \\ a_{22} &= J_y + ml^2\cos^2(\theta). \end{aligned} \quad (7)$$

B. Input Dead Zone

The unknown dead zone can be written as

$$O(u(t)) = \begin{cases} b_r(u(t) - h_r) & \text{if} \quad u(t) \geq h_r \\ 0 & \text{if} \quad h_l < u(t) < h_r \\ b_l(u(t) - h_l) & \text{if} \quad u(t) \leq h_l \end{cases} \quad (8)$$

where $u(t)$ is the dead zone input, and h_r, h_l, b_r, and b_l denote the unknown dead zone parameters. Equation (8) can be rewritten as

$$O(u(t)) = bu(t) + D(u(t)) \quad (9)$$

where

$$b = \begin{cases} b_r, & u(t) \geq 0 \\ b_l, & u(t) < 0 \end{cases}$$

and

$$D(u(t)) = \begin{cases} -b_r h_r & \text{if} \quad u(t) \geq h_r \\ -bu(t) & \text{if} \quad h_l < u(t) < h_r \\ -b_l h_l & \text{if} \quad u(t) \leq h_l \end{cases}$$

where $\|D(u(t))\| \leq \rho$, ρ is a constant, and $O(u(t)) = [O_1, O_2]^T$. For simplicity, $u(t)$ is simplified to u.

Substituting (9) into (4) yields

$$\begin{aligned} \dot{x}_2 &= A(x) + B(x)O(u) + \Delta A(x) \\ &= A(x) + B(x)bu + B(x)D(u) + \Delta A(x). \end{aligned} \quad (10)$$

C. Preliminaries

To guarantee the feasibility of a viable solution within the system under consideration, the following assumptions and lemmas are presented.

Assumption 1: An unknown positive constant B^* exists such that $\|B(x)\| \leq B^*$.

Assumption 2: The desired trajectory x_d is continuously bounded and differentiable, and its derivative $\dot{x}_d$ is both continuous and bounded.

Assumption 3: Assume $Q_1 = (K_{pp}/a_{12})$, $Q_2 = (ml^2/a_{12})$, $Q_3 = (K_{yy}/a_{22})$, $Q_4 = 2(ml^2/a_{22})$, and the aforementioned parameters are positive numbers; thus they can be expressed as follows:

$$\begin{aligned} Q_1 \approx Q_2 \approx Q_3 \approx Q_4 := l_1 \\ a_{12} \approx a_{22} \approx \hat{a}_{12} \approx \hat{a}_{22} := l_2. \end{aligned} \quad (11)$$

Assumption 4: Assume that the following inequality holds:

$$\begin{cases} k_{11} > \frac{l_1}{l_2} \\ \left(k_{11} - \frac{l_1}{l_2}\right)\left(k_{21} - \frac{l_1}{l_2} + \delta_1\right) > \delta_2 \end{cases} \quad (12)$$

where k_{11}, k_{12}, k_{21}, $k_{22} > 0$, $k_1 = k_{11} + k_{12}$, and $k_2 = k_{21} + k_{22}$. And $\delta_a = \dot{\hat{\theta}}\cos(\theta)\sin(\theta)(l_1/l_2)$, $\delta_b = \dot{\hat{\psi}}\cos^2(\theta)\sin^2(\theta)(l_1^2/4l_2^2)$.

Lemma 1 [38]: Consider a positive-definite continuous candidate Lyapunov function. If it is bounded by the initial condition $V(0)$, the following inequality holds:

$$\dot{V}(x) \le -LV(x) + C_1 \tag{13}$$

where $L > 0$ and C_1 are positive constants, and $V(x)$ remains bounded.

Lemma 2 [14]: For any constant $a > 0$ and $q \in R$, the following inequality holds:

$$0 \le |q| - \frac{q^2}{\sqrt{q^2 + a}} < \sqrt{a}. \tag{14}$$

Lemma 3 [39]: The RBFNN can approximate any unknown nonlinear function $F(X)$, and its form is

$$F(X) = W^{*T} S(X) + \eta \tag{15}$$

where $X \in \mathbb{R}^i$ and $W^{*T} \in \mathbb{R}^p$ represent the input vector and optimal weight matrix, respectively. η is the approximation error satisfying $\|\eta\| \le \bar{\eta}$, where $\bar{\eta}$ is an unknown constant. $S(X) = [s_1(X), s_2(X), \ldots, s_p(X)]^T$ is a Gaussian function vector that can be expressed as follows:

$$s_i(X) = \exp\left[\frac{-(X - c_i)^T (X - c_i)}{b_w^2}\right], i = 1, 2, \ldots, p \tag{16}$$

where c_i is the center of the receptive field, and b_w is the width of the RBFNN.

Lemma 4 [40]: Let $\beta_1(j,t)$, $\beta_2(j,t) \in R$ with $t > 0$; the following inequalities hold:

$$\beta_1(j,t)\,\beta_2(j,t) \le b_0\beta_1^2(j,t) + \frac{1}{b_0}\beta_2^2(j,t), j \in [0, R] \tag{17}$$

where b_0 denotes a positive constant.

D. Sensor Fault

The effectiveness loss fault of sensor is described as

$$\xi^f = \lambda\xi \quad \forall t > T_f \tag{18}$$

where $0 < \lambda < 1$, ξ^f denotes the value measured by the sensor, and ξ denotes the system state. T_f denotes the time at which a fault occurs.

Remark 1: When describing the sensor fault, if $0 < \lambda < 1$, then a sensor-gain fault exists in the system. Conversely, $\lambda = 1$ indicates that there is no sensor fault in the system and the sensor's effectiveness remains unaffected.

Considering the presence of sensor faults in (18) and (10), we rewrite (3)–(5) as

$$\dot{x}_1 = x_2 \tag{19}$$

$$\begin{aligned}\dot{x}_2 &= A(x) + B(x)O(u) + \Delta A(x)\\ &= A(x) + B(x)O(u) + \Delta A(\hat{x}) + \delta_1\\ &= A(x) + B(x)bu + \Xi\end{aligned} \tag{20}$$

$$y^f = \lambda x_1 \tag{21}$$

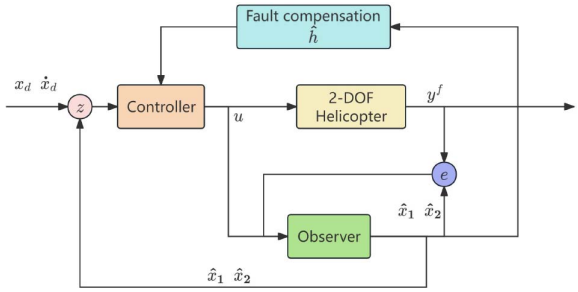

Fig. 2. Control framework.

where $\Xi = B(x)D(u) + \Delta A = B(x)D(u) + \Delta A(\hat{x}) + \delta_1$ and $\delta_1 = \Delta A(x) - \Delta A(\hat{x})$

To mitigate the impact of sensor faults on the system, the proposed state observer was designed to correct the system states and introduce adaptive parameters to estimate the faults in real time, providing compensation information for subsequent controller design. The design of the state observer is as follows [41]:

$$\dot{\hat{x}}_1 = \hat{x}_2 + P_1(\hat{h}y^f - \hat{x}_1) \tag{22}$$

$$\begin{aligned}\dot{\hat{x}}_2 &= A(\hat{x}) + B(\hat{x})O(u) + P_2(\hat{h}y^f - \hat{x}_1) + \Delta\hat{A}(\hat{x})\\ &= A(\hat{x}) + B(\hat{x})(bu + D(u)) + P_2(\hat{h}y^f - \hat{x}_1) + \Delta\hat{A}(\hat{x})\\ &= A(\hat{x}) + B(\hat{x})bu + P_2(\hat{h}y^f - \hat{x}_1) + B(\hat{x})D(u) + \Delta\hat{A}(\hat{x})\\ &= A(\hat{x}) + B(\hat{x})bu + P_2(\hat{h}y^f - \hat{x}_1) + \sigma\end{aligned} \tag{23}$$

$$\hat{y} = \hat{x}_1 \tag{24}$$

where $\hat{h}$ is the estimation of h, and $h = (1/\lambda)$, $\hat{\lambda} = (1/\hat{h})$. And $\sigma = \hat{B}D(u) + \Delta\hat{A}(\hat{x})$, $P_1 = \mathrm{diag}[P_{11}, P_{12}] \in \mathbb{R}^{2\times 2}$, $P_2 = \mathrm{diag}[P_{21}, P_{22}] \in \mathbb{R}^{2\times 2}$

Remark 2: Here, we introduce a parameter h and utilize its observed value $\hat{h}$ for fault compensation. Using the parameter $\hat{h}$, sensor faults can be detected in real time, providing essential information for the controller's compensation. Therefore, the parameter $\hat{h}$ is crucial for the controller's compensation because it directly affects the performance of the observer and the overall tracking capability of the system.

III. Control Design

This section elucidates the controller design methodology based on the closed-loop control structure illustrated in Fig. 2. The principles are introduced in the following two sections.

A. Observer Stability Analysis

By combining with (6), the observer in (22) and (23) can be rewritten as

$$\begin{aligned}\ddot{\hat{\theta}} &= \frac{\hat{a}_{11}}{\hat{a}_{12}} + \frac{K_{pp}}{\hat{a}_{12}}O_1 + \frac{K_{py}}{\hat{a}_{12}}O_2 + P_{21}(\hat{h}\lambda\theta - \hat{\theta}) + \Delta\hat{A}(\hat{x})(1)\\ \ddot{\hat{\psi}} &= \frac{\hat{a}_{21}}{\hat{a}_{22}} + \frac{K_{yp}}{\hat{a}_{22}}O_1 + \frac{K_{yy}}{\hat{a}_{22}}O_2 + P_{22}(\hat{h}\lambda\psi - \hat{\psi}) + \Delta\hat{A}(\hat{x})(2).\end{aligned} \tag{25}$$

Since $\Delta A(\hat{x})$ denotes the model uncertainty of the helicopter system, it can be estimated using the RBFNN from Lemma 3. Then, we have

$$\begin{aligned}\Delta A(\hat{x}) &= W^{*T} S(\hat{X}_1) + \eta_1 \\ \Delta \hat{A}(\hat{x}) &= \hat{W}^T S(\hat{X}_1)\end{aligned} \tag{26}$$

where W^* represents the optimal weight matrix, $\hat{X}_1 = [\hat{x}_1, \hat{x}_2]^T$ is the input to the RBFNN, and η_1 is the estimation error satisfying $\|\eta_1\| \le \bar{\eta}_1$, where $\bar{\eta}_1$ is an unknown positive constant.

Furthermore, we set $W^* = [W_1^*, W_2^*]^T$ and $\hat{W} = [\hat{W}_1, \hat{W}_2]^T$, and the approximation error of the RBFNN denoted by $\tilde{W}_i = \hat{W}_i - W_i^*$, $i = 1, 2$. We then define the observer's estimation error as

$$\begin{aligned}&e_1 = \theta - \hat{\theta} \quad e_2 = \psi - \hat{\psi} \quad e_3 = \dot{\theta} - \dot{\hat{\theta}} \\ &e_4 = \dot{\psi} - \dot{\hat{\psi}} \quad \tilde{h} = h - \hat{h}.\end{aligned} \tag{27}$$

From (19)–(21), (25), and (27), we obtain the error system of the observer as

$$\begin{aligned}\dot{e}_1 &= e_3 - P_{11}e_1 + P_{11}\tilde{h}y^f(1) \\ \dot{e}_2 &= e_4 - P_{12}e_2 + P_{12}\tilde{h}y^f(2) \\ \dot{e}_3 &= R_1 - P_{21}e_1 + P_{21}\tilde{h}y^f(1) - \tilde{W}_1^T S(\hat{X}_1) + \Xi_1 \\ \dot{e}_4 &= R_2 - P_{22}e_2 + P_{22}\tilde{h}y^f(2) - \tilde{W}_2^T S(\hat{X}_1) + \Xi_2\end{aligned} \tag{28}$$

where

$$\begin{aligned}R_1 &= \frac{a_{11}}{a_{12}} + \frac{K_{pp}}{a_{12}}O_1 + \frac{K_{py}}{a_{12}}O_2 - \frac{\hat{a}_{11}}{\hat{a}_{12}} + \frac{K_{pp}}{\hat{a}_{12}}O_1 + \frac{K_{py}}{\hat{a}_{12}}O_2 \\ R_2 &= \frac{a_{21}}{a_{22}} + \frac{K_{yp}}{a_{22}}O_1 + \frac{K_{yy}}{a_{22}}O_2 - \frac{\hat{a}_{21}}{\hat{a}_{22}} + \frac{K_{yp}}{\hat{a}_{22}}O_1 + \frac{K_{yy}}{\hat{a}_{22}}O_2 \\ \Xi_1 &= \delta_1(1) + \eta_1(1) \\ \Xi_2 &= \delta_1(2) + \eta_1(2)\end{aligned} \tag{29}$$

and $\|\Xi_1\| \le \bar{\Xi}_1$, $\|\Xi_2\| \le \bar{\Xi}_2$, where $\bar{\Xi}_1$ and $\bar{\Xi}_2$ are constants.

To evaluate the properties of the state observer (22)–(24), we consider the Lyapunov candidate

$$\begin{aligned}V_0 = &\frac{1}{2}{e_1}^2 + \frac{1}{2}{e_2}^2 + \frac{1}{2}{e_3}^2 + \frac{1}{2}{e_4}^2 + \frac{1}{2r_1}\tilde{h}^2 \\ &+ \mathrm{tr}\left\{\frac{1}{2}\tilde{W}_1^T\Lambda_1^{-1}\tilde{W}_1\right\} + \mathrm{tr}\left\{\frac{1}{2}\tilde{W}_2^T\Lambda_2^{-1}\tilde{W}_2\right\}.\end{aligned} \tag{30}$$

The derivative of V_0 yields

$$\begin{aligned}\dot{V}_0 = &e_1e_3 - P_{11}{e_1}^2 + P_{11}e_1\tilde{h}y^f(1) \\ &+ e_2e_4 - P_{12}{e_2}^2 + P_{12}e_2\tilde{h}y^f(2) + e_3\Xi_1 + e_4\Xi_2 \\ &+ e_3R_1 - e_3(P_{21}e_1 - P_{21}\tilde{h}y^f(1)) - e_3\tilde{W}_1^T S(\hat{X}_1) \\ &+ e_4R_2 - e_4(P_{22}e_2 - P_{22}\tilde{h}y^f(2)) - e_4\tilde{W}_2^T S(\hat{X}_1) \\ &- \frac{1}{r_1}\tilde{h}\dot{\hat{h}} + \mathrm{tr}\{\tilde{W}_1^T\Lambda_1^{-1}\dot{\hat{W}}_1\} + \mathrm{tr}\{\tilde{W}_2^T\Lambda_2^{-1}\dot{\hat{W}}_2\}.\end{aligned} \tag{31}$$

From (11) and (12), we obtain

$$\begin{aligned}e_3R_1 + e_4R_2 \le\ & e_3\left(\frac{a_{11}}{a_{12}} - \frac{\hat{a}_{11}}{\hat{a}_{12}} - k_1e_3^2\right) \\ &+ e_4\left(\frac{a_{21}}{a_{22}} - \frac{\hat{a}_{21}}{\hat{a}_{22}} - k_2e_4^2\right) \\ =\ & e_3\left(\frac{l_1}{l_2}e_3 - k_1e_3\right) + e_4\left(\frac{l_1}{l_2}e_4 - k_2e_4\right) \\ &+ \frac{l_1}{l_2}\cos(\theta)\sin(\theta)(e_3e_4\dot{\hat{\psi}} - e_4^2\dot{\hat{\theta}}) \\ =\ & -\begin{bmatrix}e_3 & e_4\end{bmatrix}F\begin{bmatrix}e_3 \\ e_4\end{bmatrix} - k_{12}e_3^2 - k_{22}e_4^2 \\ \le\ & -k_{12}e_3^2 - k_{22}e_4^2\end{aligned} \tag{32}$$

where

$$F = \begin{bmatrix}k_{11} - \frac{l_1}{l_2} & \frac{l_1}{2l_2}\dot{\hat{\psi}}\cos(\theta) \\ \frac{l_1}{2l_2}\dot{\hat{\psi}}\cos(\theta) & k_{21} - \frac{l_1}{l_2} + \frac{l_1}{l_2}\dot{\hat{\theta}}\cos(\theta)\sin(\theta)\end{bmatrix}.$$

Then, the following updated laws are designed:

$$\begin{aligned}\dot{\hat{h}} = &r_1(P_{11}e_1y^f(1) + P_{12}e_2y^f(2)) + P_{21}e_3y^f(1) \\ &+ P_{22}e_4y^f(2)) - r_2\hat{h}\end{aligned} \tag{33}$$

$$\dot{\hat{W}}_1 = \Lambda_1(S(\hat{X}_1)e_3 - \lambda_1\hat{W}_1) \tag{34}$$

$$\dot{\hat{W}}_2 = \Lambda_2(S(\hat{X}_1)e_4 - \lambda_2\hat{W}_2). \tag{35}$$

Considering (30)–(35), we obtain

$$\begin{aligned}\dot{V}_0 \le\ & e_1e_3 - P_{11}{e_1}^2 + e_2e_4 - P_{12}{e_2}^2 - P_{21}e_1e_3 \\ &- P_{22}e_2e_4 - k_{12}e_3^2 - k_{22}e_4^2 - \frac{r_2}{r_1}\tilde{h}^2 + \frac{r_2}{r_1}\tilde{h}h \\ &- \lambda_1\mathrm{tr}\{\tilde{W}_1^T\hat{W}_1\} - \lambda_2\mathrm{tr}\{\tilde{W}_2^T\hat{W}_2\} + e_3\Xi_1 + e_4\Xi_2.\end{aligned} \tag{36}$$

According to Young's inequality, we get

$$\frac{r_2}{r_1}\tilde{h}h \le \frac{r_2}{\xi_1 r_1}\tilde{h}^2 + \frac{\xi_1 r_2}{r_1}h^2 \tag{37}$$

$$-\lambda_1\,\mathrm{tr}\left\{\tilde{W}_1^T\hat{W}_1\right\} \le -\frac{\lambda_1}{2}\|\tilde{W}_1\|_F^2 + \frac{\lambda_1}{2}\|W_1^*\|_F^2 \tag{38}$$

$$-\lambda_2\,\mathrm{tr}\left\{\tilde{W}_2^T\hat{W}_2\right\} \le -\frac{\lambda_2}{2}\|\tilde{W}_2\|_F^2 + \frac{\lambda_2}{2}\|W_2^*\|_F^2 \tag{39}$$

$$e_3\Xi_1 \le \frac{1}{2}e_3^2 + \frac{1}{2}\bar{\Xi}_1^2, \quad e_4\Xi_2 \le \frac{1}{2}e_4^2 + \frac{1}{2}\bar{\Xi}_2^2 \tag{40}$$

where $\xi_1 > 0$ is an unknown constant.

Let $P_{21} = P_{22} = 1$, $P_{11} > 0$, and $P_{12} > 0$. Combining this with (37)–(40), (36) can be rewritten as

$$\begin{aligned}\dot{V}_0 \le\ & -P_{11}{e_1}^2 - P_{12}{e_2}^2 - \left(k_{12} - \frac{1}{2}\right)e_3^2 - \left(k_{22} - \frac{1}{2}\right)e_4^2 \\ &- \frac{r_2}{r_1}\left(1 - \frac{1}{\xi_1}\right)\tilde{h}^2 - \frac{\lambda_1}{2}\|\tilde{W}_1\|_F^2 - \frac{\lambda_2}{2}\|\tilde{W}_2\|_F^2 \\ &+ \frac{\xi_1 r_2}{r_1}h^2 + \frac{\lambda_1}{2}\|W_1^*\|_F^2 + \frac{\lambda_2}{2}\|W_2^*\|_F^2 + \frac{1}{2}\bar{\Xi}_1^2 + \frac{1}{2}\bar{\Xi}_2^2 \\ \le\ & -\mu_1V_0 + c_1\end{aligned} \tag{41}$$

where

$$\begin{aligned}\mu_1 = \min\Bigg\{&2P_{11}, 2P_{12}, 2\left(k_{12} - \frac{1}{2}\right), 2\left(k_{22} - \frac{1}{2}\right), \\ &2r_2\left(1 - \frac{1}{\xi_1}\right), \frac{\lambda_1}{\lambda_{\max}(\Lambda_1^{-1})}, \frac{\lambda_2}{\lambda_{\max}(\Lambda_2^{-1})}\Bigg\}\end{aligned}$$

and

$$\begin{aligned}c_1 = &\frac{\xi_1 r_2}{r_1}h^2 + \frac{\xi_1 r_2}{r_1}h^2 + \frac{\lambda_1}{2}\|W_1^*\|_F^2 \\ &+ \frac{\lambda_2}{2}\|W_2^*\|_F^2 + \frac{1}{2}\bar{\Xi}_1^2 + \frac{1}{2}\bar{\Xi}_2^2.\end{aligned}$$

To ensure that $\mu_1 > 0$, it is necessary to choose appropriate parameters such that $2P_{11} > 0$, $2P_{12} > 0$, $2(k_{12} - (1/2)) > 0$, $2(k_{22} - (1/2)) > 0$, $2r_2(1 - (1/\xi_1)) > 0$,$(\lambda_1/\lambda_{\max}(\Lambda_1^{-1})) > 0$,$(\lambda_2/\lambda_{\max}(\Lambda_2^{-1})) > 0$.

Subsequently, multiplying (30) by $e^{\rho_1 t}$ integrating over t, we can obtain

$$V_0 \leq \left[V_0(0) - \frac{c_1}{\mu_1}\right] e^{-\rho_1 t} + \frac{c_1}{\mu_1} \leq V_0(0) + \frac{c_1}{\mu_1}. \tag{42}$$

Remark 3: From (30), (41), and (42), it is evident that by selecting appropriate parameters, the Lyapunov function V_0 is positive definite and $\dot{V}_0$ is negative semidefinite. In other words, the observer can accurately estimate the state of the system and the sensor fault values when sensor faults occur.

B. Controller Design and Stability Analysis

Because of sensor faults, the state variables of the system are not directly accessible to the controller design. Consequently, the following coordinate transformation is defined:

$$z_1 = x_1 - x_d = \hat{h}y^f - x_d + \tilde{h}y^f \tag{43}$$

$$z_2 = \hat{x}_2 - \alpha_1 \tag{44}$$

where α_1 is the virtual control law.

According to (19), (43), (44), and $x_2 = \hat{x}_2 + e_5$, the derivative of z_1 can be computed by

$$\dot{z}_1 = x_2 - \dot{x}_d = z_2 + \alpha_1 + e_5 - \dot{x}_d \tag{45}$$

where $e_5 = [e_3, e_4]^T$.

Subsequently, the following Lyapunov candidate function is introduced:

$$V_1 = \frac{1}{2} z_1^T z_1. \tag{46}$$

And the derivative of V_1 is given by

$$\dot{V}_1 = z_1^T (z_2 + \alpha_1 + e_5 - \dot{x}_d) \tag{47}$$

where α_1 denotes the virtual controller, designed as follows:

$$\alpha_1 = -c_1 z_1 - e_5 + \dot{x}_d \tag{48}$$

where $c_1 > 0$ is a control gain.

Substituting (48) into (47) yields

$$\dot{V}_1 = z_1^T z_2 - c_1 z_1^T z_1. \tag{49}$$

Combining (23) and (44), we obtain

$$\dot{z}_2 = A(\hat{x}) + B(\hat{x})bu + \sigma + P_2(\hat{h}y^f - \hat{x}_1) - \dot{\alpha}_1. \tag{50}$$

Since σ is an unknown nonlinear function, it can be estimated using the RBFNN from Lemma 3. Then, we have

$$\sigma = W_3^{*T} S(X) + \eta_3 \tag{51}$$

where W^* represents the optimal weight matrix, and $X = [x_1, x_2, \hat{x}_1, \hat{x}_2]^T$ is the input vector. η is the estimation error satisfying $\|\eta_3\| \leq \bar{\eta}_3$, where $\bar{\eta}_3$ is an unknown positive constant.

Combining (50) and (51), we have

$$\dot{z}_2 = A(\hat{x}) + B(\hat{x})bu + W_3^{*T} S(X) + \eta_3 + P_2(\hat{h}y^f - \hat{x}_1) - \dot{\alpha}_1. \tag{52}$$

We introduce an auxiliary variable γ, which is defined as follows:

$$\gamma = A(\hat{x}) + P_2(\hat{h}y^f - \hat{x}_1) + \hat{W}_3^T S(X) - \dot{\alpha}_1 - c_2 z_2 + z_1 \tag{53}$$

where c_2 is a positive control gain. Then, we obtain

$$z_2^T \dot{z}_2 = z_2^T B(\hat{x})bu + z_2^T \gamma - z_2^T \tilde{W}_3^T S(X) - c_2 z_2^T z_2 + z_2^T \eta_3. \tag{54}$$

Since b is bounded, we have $\kappa = \inf_{t \geq 0} b$ and $\zeta = (1/\kappa)$. Subsequently, we propose the following AFTC strategy:

$$u = -\hat{B}^{-1} z_2 \frac{\hat{\zeta}^2 \gamma^T \gamma}{\sqrt{\hat{\zeta}^2 z_2^T z_2 \gamma^T \gamma + \epsilon}} \tag{55}$$

where is ϵ a small constant.

Moreover, we define $\tilde{\zeta} = \zeta - \hat{\zeta}$ and $\tilde{W}_3 = \hat{W}_3 - W_3^*$, the updating laws of $\dot{\hat{\zeta}}$ and $\dot{\hat{W}}$ are given by

$$\dot{\hat{\zeta}} = \lambda_3 (z_2^T \gamma - \sigma_3 \hat{\zeta}) \tag{56}$$

$$\dot{\hat{W}}_3 = \lambda_4 (S(X) z_2^T - \sigma_4 \hat{W}_3) \tag{57}$$

where λ_3, σ_3, and σ_4 are the designed parameters, and λ_4 denotes a constant gain matrix.

The following Lyapunov function is designed:

$$V_2 = V_1 + \frac{1}{2} z_2^T z_2 + \frac{1}{2} \mathrm{tr}\{\tilde{W}_3^T \lambda_4^{-1} \tilde{W}_3\} + \frac{\kappa}{2\lambda_3} \tilde{\zeta}^2. \tag{58}$$

From (55) and Lemma 2, we have

$$\begin{aligned} z_2^T \hat{B} b u = & - \frac{z_2^T \hat{B} b \hat{B}^{-1} z_2 \hat{\zeta}^2 \gamma^T \gamma}{\sqrt{\hat{\zeta}^2 z_2^T z_2 \gamma^T \gamma + \epsilon}} \\ \leq & - \frac{\kappa z_2^T z_2 \hat{\zeta}^2 \gamma^T \gamma}{\sqrt{\hat{\zeta}^2 z_2^T z_2 \gamma^T \gamma + \epsilon}} \\ \leq & \kappa(\sqrt{\epsilon} - \hat{\zeta} z_2^T \gamma). \end{aligned} \tag{59}$$

By combining (17), (49), and (56)–(59), we derive $\dot{V}_2$

$$\begin{aligned} \dot{V}_2 = & - c_1 z_1^T z_1 - c_2 z_2^T z_2 + z_2^T B(\hat{x}) b u - z_2^T \tilde{W}_3 S(X) \\ & + z_2^T \eta_3 + z_2^T \gamma + \mathrm{tr}\{\tilde{W}_3^T \lambda_4^{-1} \dot{\tilde{W}}_3\} - \frac{\kappa}{\lambda_3} \tilde{\zeta} \dot{\tilde{\zeta}} \\ \leq & - c_1 z_1^T z_1 - c_2 z_2^T z_2 - \sigma_4 tr\{\tilde{W}_3^T \hat{W}_3\} \\ & + \kappa \sigma_3 \tilde{\zeta} \zeta - \kappa \sigma_3 \tilde{\zeta}^2 + z_2^T \eta_3 + \kappa \sqrt{\epsilon} \end{aligned} \tag{60}$$

where $z_2^T \eta_3 \leq (1/2) z_2^T z_2 + (1/2) \bar{\eta}_3^2$.

By using Young's inequality in conjunction with (17), we derive

$$-\sigma_4 \mathrm{tr}\{\tilde{W}_3^T \hat{W}_3\} \leq - \frac{\sigma_4}{2} \|\tilde{W}_3\|^2 + \frac{\sigma_4}{2} \|W_3^*\|^2 \tag{61}$$

$$\kappa \sigma_3 \tilde{\zeta} \zeta \leq \frac{\kappa \sigma_3}{a_1} \tilde{\zeta}^2 + a_1 \kappa \sigma_3 \zeta^2 \tag{62}$$

where $a_1 > 0$ is a constant.

Substituting (61) and (62) into (60) yields

$$\dot{V}_2 \leq - c_1 z_1^T z_1 - \left(c_2 - \frac{1}{2}\right) z_2^T z_2 - \kappa \sigma_3 \left(1 - \frac{1}{a_1}\right) \tilde{\zeta}^2$$

$$-\frac{\sigma_4}{2}\|\tilde{W}_3\|^2+\frac{\sigma_4}{2}\|W_3^*\|^2+a_1\kappa\sigma_3\zeta^2+\frac{1}{2}\bar{\eta}_3^2+\kappa\sqrt{\epsilon}$$
$$\leq -\mu_2 V_2+c_2 \tag{63}$$

where

$$\mu_2=\min\left\{2\lambda_{\min}(c_1),2\lambda_{\min}\left(c_2-\frac{1}{2}I_{2\times 2}\right),\right.$$
$$\left.\frac{\sigma_4}{\lambda_{\max}(\lambda_4^{-1})},2\lambda_3\sigma_3\lambda_{\min}\left(1-\frac{1}{a_1}\right)\right\}$$

and

$$c_2=\frac{\sigma_4}{2}\|W_3^*\|^2+a_1\kappa\sigma_3\zeta^2+\frac{1}{2}\bar{\eta}_3^2+\kappa\sqrt{\epsilon}$$

To ensure that $\mu_2>0$, it is necessary to choose appropriate parameters such that $2\lambda_{\min}(c_1)>0$, $2\lambda_{\min}(c_2-(1/2)I_{2\times 2})>0$, $(\sigma_4/\lambda_{\max}(\lambda_4^{-1}))$ and $2\lambda_3\sigma_3\lambda_{\min}(1-(1/a_1))>0$

Subsequently, multiplying (63) by $e^{\rho_1 t}$ and integrating over t yields

$$V_2\leq\left[V_2(0)-\frac{c_2}{\mu_2}\right]e^{-\rho_1 t}+\frac{c_2}{\mu_2}\leq V_2(0)+\frac{c_2}{\mu_2}. \tag{64}$$

Therefore, all signals of the closed-loop control system are semiglobally consistent and bounded.

IV. Simulations

Two numerical simulations are conducted to assess the effectiveness of the proposed AFTC strategy. First, the fault parameter is set to $\lambda=0.6$, and the simulation results are used to validate the accuracy of the proposed observer. Next, the proposed control method is compared with a control method that uses an adaptive compensation scheme to approximate dead-zone disturbances [40]. Finally, control situations with and without fault compensation are further explored.

In the simulation, the parameters of the helicopter system are set as follows: $m=1.0750\,\text{kg}$, $G=9.81\,\text{m/s}^2$, $l=0.0025\,\text{m}$, $D_{pp}=0.0071\,\text{N/V}$, $D_{yy}=0.0220\,\text{N/V}$, $k_{pp}=0.0011\,\text{N}\cdot\text{m/V}$, $K_{py}=0.0021\,\text{N}\cdot\text{m/V}$, $K_{yp}=-0.0027\,\text{N}\cdot\text{m/V}$, $K_{yy}=0.0022\,\text{N}\cdot\text{m/V}$, $J_y=0.0238\,\text{kg}\cdot\text{m}^2$, and $J_p=0.0232\,\text{kg}\cdot\text{m}^2$. The initial states and desired trajectories are set to $x_1(0)=[0,0]^T$, $x_2(0)=[0,0]^T$, and $x_d=[0.28\sin(t),0.33\sin(t)]^T$. The dead-zone parameters are given as $b_r=1.5$, $b_l=1.45$, $h_l=[-0.4,-0.4]^T$, and $h_r=[0.5,0.5]^T$.

A. Verification of Observer Accuracy

To verify the accuracy of the proposed observer, the observer parameters are set as $P_{11}=500$, $P_{12}=500$, $P_{21}=1$, and $P_{22}=1$. The other design parameters are set to $\Lambda_1=15I_{256\times 256}$, $\Lambda_2=15I_{256\times 256}$, $\lambda_1=0.1$, and $\lambda_2=0.1$. r_1 and r_2 are the adaptive tuning parameters in the fault-detection observer that determine the convergence rate and stability of the estimation law. Three cases are designed for simulation validation to verify the influence of different parameters. In Case 1, $r_1=0.8$, $r_2=0.001$; $r_1=0.8$, $r_2=0.01$; and $r_1=0.8$, $r_2=0.1$ are considered. In Case 2, $r_1=0.08$, $r_2=0.01$; $r_1=0.8$, $r_2=0.01$; and $r_1=1.8$, $r_2=0.01$ are used. In Case 3, when $r_1=0.8$ and $r_2=0.01$, the fault occurrence times

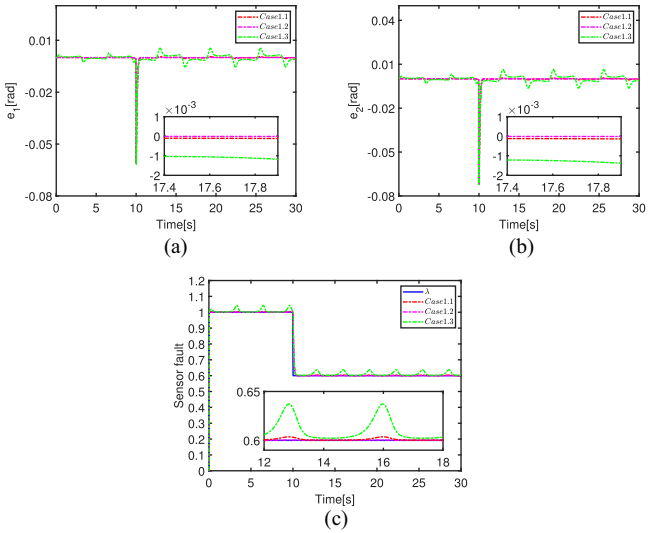

Fig. 3. Case 1: accuracy of observer in simulation. (a) Trajectory of e_1. (b) Trajectory of e_2. (c) Fault estimation $\hat{\lambda}$.

$T_f=10s$ and $T_f=15s$ are considered. In both Cases 1 and 2, a fault occurred at $T_f=10$ s.

The simulation results are shown in Fig. 3–5. Cases 1.1–1.3 correspond to the three parameter settings described in Case 1, and Cases 2.1–2.3, and Cases 3.1 and 3.2 follow the same numbering pattern, corresponding to the parameter configurations in Cases 2 and 3, respectively. As illustrated in Figs. 3(a) and (b) and 4(a) and (b), the observer accurately estimate the actual system states before the occurrence of sensor faults. When a sensor fault is introduced at $t=10s$, a short and slight deviation was observed between the estimated and actual states. However, the observer responded rapidly and reestablished accurate state estimation. Figs. 3(c) and 4(c) further show that the proposed observer can quickly and precisely estimate sensor faults. Moreover, Figs. 3 and 4 demonstrate that maintaining a constant r_1 while gradually increasing r_2 leads to an initial improvement in observer performance, followed by degradation when r_2 exceeds a certain value. Similarly, with a fixed r_2, progressively increasing r_1 first enhances then reduces observer effectiveness. Comparative results indicate that the observer achieves optimal performance when $r_1=0.8$ and $r_2=0.01$.

In addition, as shown in Fig. 5, when the fault occurred at $t=10$ s or $t=15$ s, the observer accurately estimates both the system states and the sensor faults.

B. Comparison Between the Proposed Control and Adaptive Dead-Zone Disturbance Compensation Control

To verify the effectiveness of the proposed control method, we compare it to a control strategy that employs adaptive parameters to approximate dead-zone disturbances. The control gains are set as $c_1=[40,40]^T$ and $c_2=[50,50]^T$, and the parameters are chosen as $\lambda_3=0.0018$, $\sigma_3=0.001$, $\lambda_4=1.5I_{256\times 256}$, $\sigma_4=0.01$, and $\epsilon=0.25$. The remaining parameters are identical to those in Case A. The adaptive dead-zone disturbance compensation controller is given as follows. Except for $d_1=0.25$, $\lambda_5=1.5$, and $\sigma_5=0.01$, the parameters of the

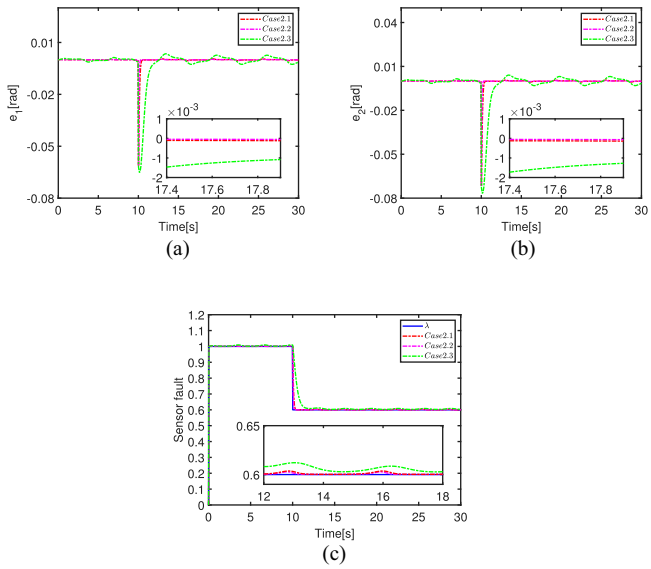

Fig. 4. Case 2: accuracy of observer in simulation. (a) Trajectory of e_1. (b) Trajectory of e_2. (c) Fault estimation $\hat{\lambda}$.

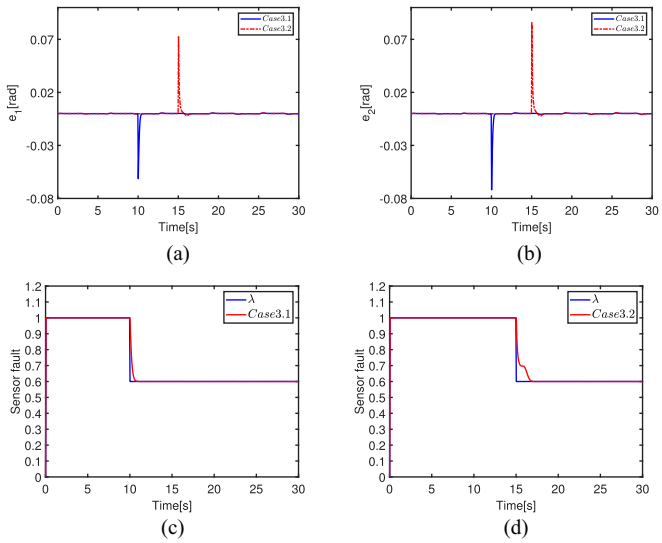

Fig. 5. Case 3: accuracy of observer in simulation. (a) Trajectory of e_1. (b) Trajectory of e_2. (c) Fault estimation $\hat{\lambda}$. (d) Fault estimation $\hat{\lambda}$.

adaptive dead-zone disturbance compensation controller are consistent with those of the proposed control method

$$u = -\hat{B}^{-1} z_2 \frac{\hat{\zeta}^2 \gamma_1^T \gamma_1}{\sqrt{\hat{\zeta}^2 z_2^T z_2 \gamma_1^T \gamma_1 + \epsilon}} \tag{65}$$

where

$$\gamma = A(\hat{x}) + P_2(\hat{h}y^f - \hat{x}_1) - \dot{\alpha}_1 - c_2 z_2 + z_1 + \hat{W}^T S(\hat{X}_1) + \tanh\left(\frac{z_2}{d_1}\right)\hat{\Omega}_f. \tag{66}$$

$\Omega = B(\hat{x})D(u)$ and $\|\Omega\| \le \Omega_f$, where Ω_f is an unknown positive constant. The updating law for $\hat{\Omega}_f$ is

$$\dot{\hat{\Omega}}_f = \lambda_5 \left(z_2^T \tanh\left(\frac{z_2}{d_1}\right) - \sigma_5 \hat{\Omega}_f \right). \tag{67}$$

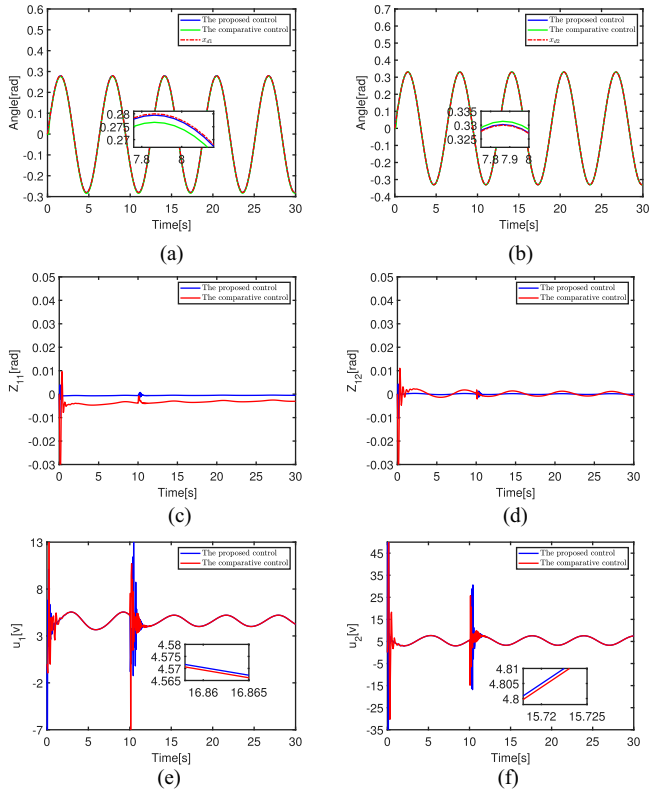

Fig. 6. Tracking performance of the proposed control and the comparative control. (a) Tracking response of θ. (b) Tracking response of ψ. (c) Tracking error z_{11}. (d) Tracking error z_{12}. (e) Control input u_1. (f) Control input u_1.

The simulation results are shown in Fig. 6. Fig. 6(a) and (b) illustrates the tracking performance of θ and ψ, respectively. The results demonstrate that the proposed control method achieves more accurate tracking performance compared to the comparative method. Fig. 6(c) and (d) presents the trajectories of the errors z_{11} and z_{12}, indicating that the proposed method consistently maintains smaller tracking errors. Fig. 6(e) and (f) shows the control input voltages. It can be seen that the method in [40] exhibits multiple voltage overshoot and shows instability.

C. Comparison Between the Proposed Control and Control Without Fault Compensation

To validate the feasibility of the proposed control method, we compare it with a control strategy without fault compensation, using the same parameter settings as in Case B.

The simulation results are presented in Fig. 7. Fig. 7(a) and (b) illustrates the tracking trajectories of θ and ψ. The results demonstrate that after the occurrence of faults, the control method without fault compensation fails to follow the desired trajectories, whereas the proposed method maintains an accurate tracking performance. Fig. 7(c) and (d) shows the control input voltages.

The analysis of these simulation results for Cases A, B, and C verifies the feasibility and superiority of the proposed control method.

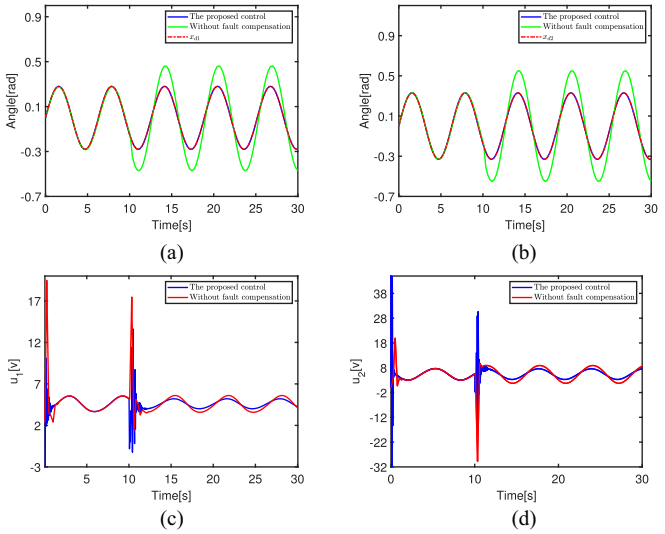

Fig. 7. Performance of the proposed control with/without fault compensation. (a) Tracking response of θ. (b) Tracking response of ψ. (c) Control input u_1. (d) Control input u_1.

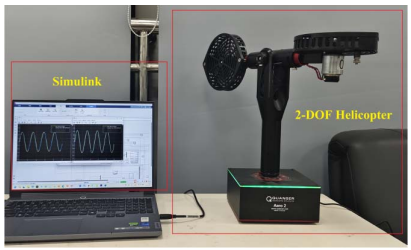

Fig. 8. Quanser Aero 2 experiment platform.

V. Experiments

To further verify the feasibility of the proposed control strategy, experimental validation is conducted using a Quanser 2-DOF helicopter platform, as shown in Fig. 8. The voltage range of the two input channels in the physical system is $[-24\text{V}, 24\text{V}]$. In addition, an industrial fan is employed in all experiments to generate wind disturbances, thereby further validating the robustness and performance of the proposed control scheme under real-world disturbance conditions. The helicopter and dead-zone parameters are set to be the same as those in the simulation. The initial states and desired trajectories are set as $x_1(0) = [0, 0]^T$, $x_2(0) = [0, 0]^T$, and $x_d = [0.28\sin(t), 0.33\sin(t)]^T$.

A. Verification of Observer Accuracy

To verify the accuracy of the proposed observer, the observer parameters are set as $P_{11} = 450$, $P_{12} = 450$, and $P_{21} = 1$ and $P_{22} = 1$. The other design parameters are set to $\Lambda_1 = 15I_{55\times55}$, $\Lambda_2 = 15I_{55\times55}$, $\lambda_1 = 0.8$, and $\lambda_2 = 0.8$. As with the simulations, we conduct comparative experiments using different values of r_1 and r_2. In Case 4, $r_1 = 0.15$, $r_2 = 0.00001$; $r_1 = 0.15$, $r_2 = 0.001$; and $r_1 = 0.15$, $r_2 = 0.001$ are considered. In Case 5, $r_1 = 0.05$, $r_2 = 0.0001$; $r_1 = 0.15$, $r_2 = 0.0001$; and $r_1 = 0.25$, $r_2 = 0.0001$ are used. In Case 6, when $r_1 = 0.15$ and $r_2 = 0.0001$, the fault occurrence times $T_f = 10s$ and $T_f = 15s$ are considered. In both Cases 1 and 2, a fault occurs at $T_f = 10$ s. In addition, the fault parameter is set to $\lambda = 0.7$.

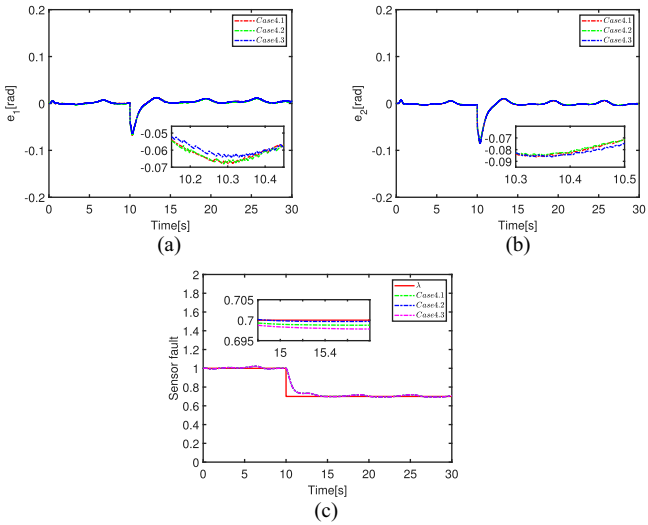

Fig. 9. Case 4: accuracy of observer in experiment. (a) Trajectory of e_1. (b) Trajectory of e_2. (c) Fault estimation $\hat{\lambda}$.

The experimental results are shown in Figs. 9–11. Cases 4.1–4.3 correspond to the three parameter configurations described in Case 4, and Cases 5.1–5.3 and 6.1 and 6.2 follow the same numbering convention, corresponding to the parameter settings in Cases 5 and 6, respectively. As shown in Figs. 9(a) and (b) and 10(a) and (b), the observer accurately estimates the actual system states before the occurrence of sensor faults. When a sensor fault is introduced at $t = 10$ s, a brief and slight deviation appears between the estimated and actual states. However, the observer quickly responds and restores an accurate state estimation. Figs. 9(c) and 10(c) further demonstrate that the proposed observer can rapidly and precisely identify the sensor faults. As can be seen from Figs. 9 and 10, consistent with the simulation results, maintaining a constant r_1 while gradually increasing r_2 leads to an initial improvement in observer performance, followed by degradation when r_2 exceeds a certain threshold. Similarly, with a fixed r_2, progressively increasing r_1 first enhances then reduces observer effectiveness. The comparative results indicate that the optimal observer performance is achieved when $r_1 = 0.15$ and $r_2 = 0.0001$. In addition, as shown in Fig. 11, when the fault occurs at $t = 10$ s and $t = 15$ s, the observer still accurately estimates both the system states and the sensor faults.

B. Comparison Between the Proposed Control and the Adaptive Dead-Zone Disturbance Compensation Control

The control gains are set to $c_1 = [18, 18]^T$ and $c_2 = [19, 19]^T$, and the parameters are set to $\lambda_3 = 0.015$, $\sigma_3 = 0.01$, $\lambda_4 = 10I_{55\times55}$, $\sigma_4 = 0.6$, and $\epsilon = 0.25$. In the adaptive dead-zone disturbance compensation controller, $\lambda_5 = 10$ and $\sigma_5 = 0.6$, while the other parameters remain consistent with those of the proposed control method.

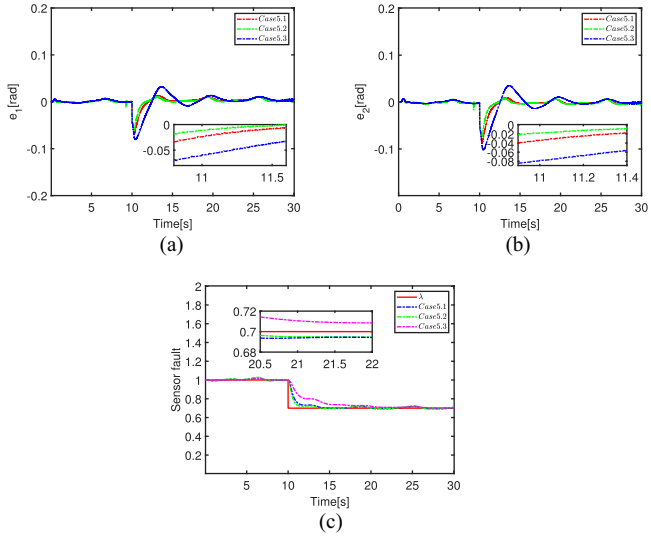

Fig. 10. Case 5: accuracy of observer in experiment. (a) Trajectory of e_1. (b) Trajectory of e_2. (c) Fault estimation $\hat{\lambda}$.

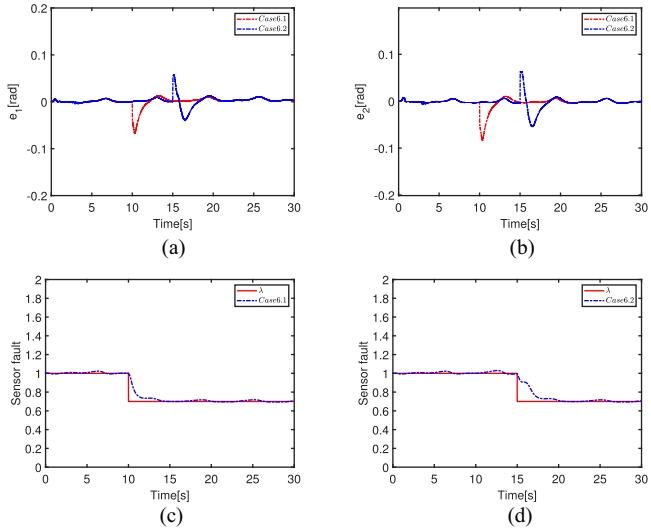

Fig. 11. Case 6: accuracy of observer in experiment. (a) Trajectory of e_1. (b) Trajectory of e_2. (c) Fault estimation $\hat{\lambda}$. (d) Fault estimation $\hat{\lambda}$.

The experimental results for the proposed control and adaptive dead-zone disturbance compensation control are shown in Fig. 12. Fig. 12(a) and (b) demonstrates the tracking performance of θ and ψ, respectively. Fig. 12(c) and (d) shows the error variations of z_{11} and z_{12}. Fig. 12(e) and (f) depicts the input voltage. The experimental results show that the proposed control method provides improved tracking performance and enhanced robustness.

C. Comparison Between the Proposed Control and the Control Without Fault Compensation

Fig. 13 presents the experimental results of the proposed control and the control without fault compensation. Fig. 13(a) and (b) demonstrates the tracking performance of θ and ψ, respectively. Fig. 13(c) and (d) shows the input voltage. The

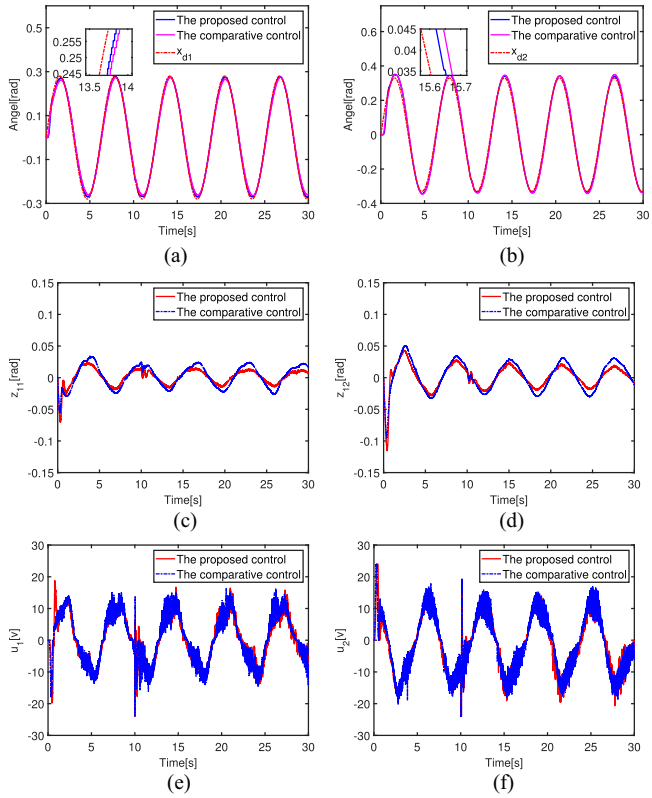

Fig. 12. Tracking performance of the proposed control and the comparative control in experiment. (a) Tracking response of θ. (b) Tracking response of ψ. (c) Tracking error z_{11}. (d) Tracking error z_{12}. (e) Control input u_1. (f) Control input u_1.

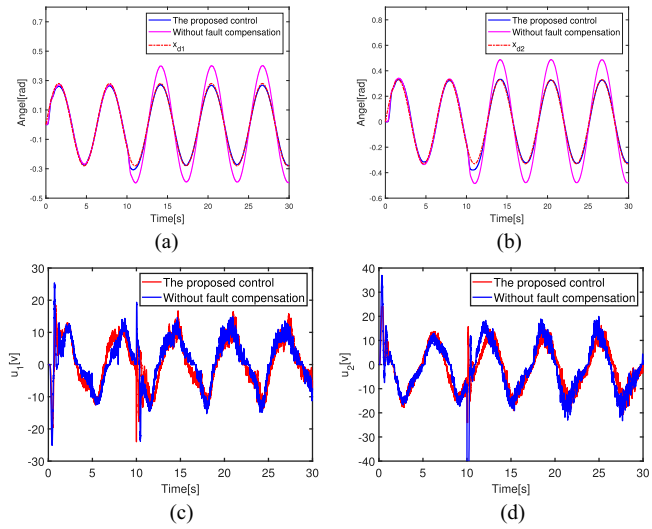

Fig. 13. Performance of the proposed control with/without fault compensation in the experiment. (a) Tracking response of θ. (b) Tracking response of ψ. (c) Control input u_1. (d) Control input u_1.

experimental results indicate that after the occurrence of sensor faults, the proposed control method responded quickly and exhibited good tracking performance. By contrast, the control method without fault compensation failed to effectively track the desired trajectory after a fault occurred.

Analysis of the experimental results further validated the effectiveness of the proposed control method.

VI. Conclusion

In this article, an neuro-learning based AFTC is proposed for a 2-DOF helicopter system with sensor gain faults and unknown dead zones. First, to address the issue of inaccurate state measurements caused by sensor faults, a state observer is designed to reconstruct the system's states, and an adaptive parameter is introduced to estimate the faults in real time. Then, an RBFNN is used to handle the uncertainties in the system. Meanwhile, bounded estimation, adaptive parameters, and RBFNN are combined to compensate for the effects of dead zones. The stability of the closed-loop system is subsequently proven using the Lyapunov method. Finally, the effectiveness of the proposed control method is validated through simulations and experiments. Future work will extend the proposed AFTC to multi–degree-of-freedom aerial platforms such as quadrotors, integrate multi-network reinforcement learning to improve data efficiency and adaptation speed, and incorporate control barrier functions to enforce safety constraints—thereby enhancing both flight performance and safety.

References

[1] Y.-C. Lai and T.-Q. Le, "Adaptive learning-based observer with dynamic inversion for the autonomous flight of an unmanned helicopter," *IEEE Trans. Aerosp. Electron. Syst.*, vol. 57, no. 3, pp. 1803–1814, Jun. 2021, doi: 10.1109/TAES.2021.3050653.

[2] G. Michieletto, A. Cenedese, L. Zaccarian, and A. Franchi, "Nonlinear control of multi-rotor aerial vehicles based on the zero-moment direction," *IFAC-PapersOnLine*, vol. 50, no. 1, pp. 13144–13149, 2017.

[3] A. Bounemeur and M. Chemachema, "General fuzzy adaptive fault-tolerant control based on nussbaum-type function with additive and multiplicative sensor and state-dependent actuator faults," *Fuzzy Sets Syst.*, vol. 468, Sep. 2023, Art. no. 108616, doi: 10.1016/j.fss.2023.108616.

[4] D. Invernizzi, M. Lovera, and L. Zaccarian, "Dynamic attitude planning for trajectory tracking in thrust-vectoring UAVs," *IEEE Trans. Autom. Control*, vol. 65, no. 1, pp. 453–460, Jan. 2020, doi: 10.1109/TAC.2019.2919660.

[5] C.-W. Kuo, C.-C. Tsai, and C.-T. Lee, "Intelligent leader-following consensus formation control using recurrent neural networks for small-size unmanned helicopters," *IEEE Trans. Syst., Man, Cybern., Syst.*, vol. 51, no. 2, pp. 1288–1301, Feb. 2021, doi: 10.1109/TSMC.2019.2896958.

[6] Z. Zhao, J. Zhang, Z. Liu, H.-X. Li, and C. Philip Chen, "Event-triggered adaptive neural fault-tolerant control for a 2-DOF helicopter system with prescribed performance," *Automatica*, vol. 162, Apr. 2024, Art. no. 111511, doi: 10.1016/j.automatica.2024.111511.

[7] H. Shen, X. Yu, H. Yan, J. H. Park, and J. Wang, "Robust fixed-time sliding mode attitude control for a 2-DOF helicopter subject to input saturation and prescribed performance," *IEEE Trans. Transport. Electrific.*, vol. 11, no. 1, pp. 1223–1233, Feb. 2025, doi: 10.1109/TTE.2024.3402316.

[8] J. Y. Yassuda, C. M. Agulhari, and E. R. P. da Silva, "Sampled-data robust control of a 2-DOF helicopter modeled using a quasi-LPV framework," *Control Eng. Pract.*, vol. 145, Apr. 2024, Art. no. 105870, doi: 10.1016/j.conengprac.2024.105870.

[9] S.-K. Kim, K. S. Kim, and C. K. Ahn, "Order reduction approach to velocity sensorless performance recovery pd-type attitude stabilizer for 2-DOF helicopter applications," *IEEE Trans. Ind. Informat.*, vol. 18, no. 10, pp. 6848–6856, Oct. 2022, doi: 10.1109/TII.2022.3143204.

[10] S. M. Schlanbusch, J. Zhou, and R. Schlanbusch, "Adaptive attitude control of a rigid body with input and output quantization," *IEEE Trans. Ind. Electron.*, vol. 69, no. 8, pp. 8296–8305, Aug. 2022, doi: 10.1109/TIE.2021.3105999.

[11] Y. Zhu, W. Zhu, J. Liu, Q.-G. Wang, and J. Yu, "Command-filtered finite-time fuzzy adaptive fault-tolerant control of output-constrainted robotic manipulators with unknown dead-zones," *IEEE Trans. Circuits Syst., II, Exp. Briefs*, vol. 70, no. 8, pp. 2939–2943, Aug. 2023, doi: 10.1109/TCSII.2023.3249188.

[12] Y.-J. Liu, S. Li, S. Tong, and C. L. P. Chen, "Adaptive reinforcement learning control based on neural approximation for nonlinear discrete-time systems with unknown nonaffine dead-zone input," *IEEE Trans. Neural Netw. Learn. Syst.*, vol. 30, no. 1, pp. 295–305, Jan. 2019, doi: 10.1109/TNNLS.2018.2844165.

[13] Y. Li, Y. Zhao, W. Liu, and J. Hu, "Adaptive fuzzy predefined-time control for third-order heterogeneous vehicular platoon systems with dead zone," *IEEE Trans. Ind. Informat.*, vol. 19, no. 9, pp. 9525–9534, Sep. 2023, doi: 10.1109/TII.2022.3221220.

[14] Z. Zhao, J. Zhang, Z. Liu, W. He, and K.-S. Hong, "Adaptive quantized fault-tolerant control of a 2-DOF helicopter system with actuator fault and unknown dead zone," *Automatica*, vol. 148, Feb. 2023, Art. no. 110792, doi: 10.1016/j.automatica.2022.110792.

[15] F. Shojaei, M. M. Arefi, A. Khayatian, and H. R. Karimi, "Observer-based fuzzy adaptive dynamic surface control of uncertain nonstrict feedback systems with unknown control direction and unknown dead-zone," *IEEE Trans. Syst., Man, Cybern. Syst.*, vol. 49, no. 11, pp. 2340–2351, Nov. 2019, doi: 10.1109/TSMC.2018.2852725.

[16] Z. Zhao, Y. Weng, Z. Liu, C. Yang, and C. L. P. Chen, "Broad reinforcement learning for adaptive control of a 2-DOF helicopter system with unknown dead zone," *IEEE Trans. Ind. Electron.*, vol. 72, no. 4, pp. 3984–3993, Apr. 2025, doi: 10.1109/TIE.2024.3454429.

[17] C. Zhu, Y. Jiang, and C. Yang, "Fixed-time neural control of robot manipulator with global stability and guaranteed transient performance," *IEEE Trans. Ind. Electron.*, vol. 70, no. 1, pp. 803–812, Jan. 2023, doi: 10.1109/TIE.2022.3156037.

[18] S. C. Yogi, V. K. Tripathi, and L. Behera, "Adaptive integral sliding mode control using fully connected recurrent neural network for position and attitude control of quadrotor," *IEEE Trans. Neural Netw. Learn. Syst.*, vol. 32, no. 12, pp. 5595–5609, Dec. 2021, doi: 10.1109/TNNLS.2021.3071020.

[19] X. Huang, C. Wen, and Y. Song, "Adaptive neural control for uncertain constrained pure feedback systems with severe sensor faults: A complexity reduced approach," *Automatica*, vol. 147, Jan. 2023, Art. no. 110701, doi: 10.1016/j.automatica.2022.110701.

[20] Z. Zhao, D. Zhang, J. Wu, Z. Liu, M. Wang, and K.-S. Hong, "Disturbance observer-based neural network control of a 2-DOF helicopter system with input saturation and output constraints," *IEEE Trans. Syst., Man, Cybern. Syst.*, vol. 55, no. 5, pp. 3152–3162, May. 2025, doi: 10.1109/TSMC.2025.3538990.

[21] L. Cao, Y. Pan, H. Liang, and C. K. Ahn, "Event-based adaptive neural network control for large-scale systems with nonconstant control gains and unknown measurement sensitivity," *IEEE Trans. Syst., Man, Cybern. Syst.*, vol. 54, no. 11, pp. 7027–7038, Nov. 2024, doi: 10.1109/TSMC.2024.3444007.

[22] M. Wan, M. Chen, and K. Yong, "Adaptive tracking control for an unmanned autonomous helicopter using neural network and disturbance observer," *Neurocomputing*, vol. 468, pp. 296–305, Jan. 2022, doi: 10.1016/j.neucom.2021.09.060.

[23] Z. Zhang, C. Wen, L. Xing, and Y. Song, "Event-triggered adaptive control for a class of nonlinear systems with mismatched uncertainties via intermittent and faulty output feedback," *IEEE Trans. Autom. Control*, vol. 68, no. 12, pp. 8142–8149, Dec. 2023, doi: 10.1109/TAC.2023.3287802.

[24] X. Wang and C. P. Tan, "Output feedback active fault tolerant control for a 3-DOF laboratory helicopter with sensor fault," *IEEE Trans. Autom. Sci. Eng.*, vol. 21, no. 3, pp. 2689–2700, Jul. 2024, doi: 10.1109/TASE.2023.3267132.

[25] M. Shen, T. Zhang, Z.-G. Wu, Q.-G. Wang, and S. Zhu, "Iterative interval estimation-based fault detection for discrete time T–S fuzzy systems," *IEEE Trans. Syst., Man, Cybern. Syst.*, vol. 53, no. 11, pp. 6966–6974, Nov. 2023, doi: 10.1109/TSMC.2023.3290042.

[26] M. Shen, Y. Ma, J. H. Park, and Q.-G. Wang, "Fuzzy tracking control for Markov jump systems with mismatched faults by iterative proportional–integral observers," *IEEE Trans. Fuzzy Syst.*, vol. 30, no. 2, pp. 542–554, Feb. 2022, doi: 10.1109/TFUZZ.2020.3041589.

[27] A. Alessandri and L. Zaccarian, "Stubborn state observers for linear time-invariant systems," *Automatica*, vol. 88, pp. 1–9, Feb. 2018, doi: 10.1016/j.automatica.2017.10.022.

[28] X. Wang, Y. Wang, Z. Zhang, X. Wang, and R. Patton, "Sensor fault tolerant control for a 3-DOF helicopter considering detectability loss," *IEEE Trans. Circuits Syst. I, Reg. Papers*, vol. 70, no. 10, pp. 4112–4125, Oct. 2023, doi: 10.1109/TCSI.2023.3303153.

[29] X. Wang, "Active fault tolerant control for unmanned underwater vehicle with sensor faults," *IEEE Trans. Instrum. Meas.*, vol. 69, no. 12, pp. 9485–9495, Dec. 2020, doi: 10.1109/TIM.2020.3003108.

[30] M. Shen, C. Wang, Q.-G. Wang, H. Yan, G. Zong, and Z. H. Zhu, "Fault-tolerant synchronization control of switched complex networks by a proportional-integral intermediate observer approach," *IEEE Trans. Cybern.*, vol. 55, no. 10, pp. 4689–4698, Oct. 2025, doi: 10.1109/TCYB.2025.3591393.

[31] W. Wu, Y. Kang, and L. Yao, "Learning observer based fault diagnosis and fault tolerant control for manipulators with sensor fault," in *Proc. CAA Symp. Fault Detection, Supervision Saf. Tech. Processes (SAFEPROCESS)*, 2019, pp. 53–58, doi: 10.1109/SAFEPROCESS45799.2019.9213440.

[32] M. M. Seron and J. A. De Doná, "Robust fault estimation and compensation for LPV systems under actuator and sensor faults," *Automatica*, vol. 52, pp. 294–301, Feb. 2015, doi: 10.1016/j.automatica.2014.12.003.

[33] S. Zeghlache, T. Benslimane, and A. Bouguerra, "Active fault tolerant control based on interval type-2 fuzzy sliding mode controller and non linear adaptive observer for 3-DOF laboratory helicopter," *ISA Trans.*, vol. 71, Part 2, pp. 280–303, Nov. 2017, doi: 10.1016/j.isatra.2017.09.006.

[34] A. Bounemeur and M. Chemachema, "Robust fuzzy adaptive fault-tolerant control for a class of second-order nonlinear systems," *Int. J. Adapt. Control Signal Process.*, vol. 39, pp. 15–30, Jan. 2025, doi: 10.1002/acs.3916.

[35] A. Bounemeur, M. Chemachema, and N. Essounbouli, "Indirect adaptive fuzzy fault-tolerant tracking control for MIMO nonlinear systems with actuator and sensor failures," *ISA Trans.*, vol. 79, pp. 45–61, Aug. 2018, doi: 10.1016/j.isatra.2018.04.014.

[36] D. Zhai, L. An, J. Dong, and Q. Zhang, "Output feedback adaptive sensor failure compensation for a class of parametric strict feedback systems," *Automatica*, vol. 97, pp. 48–57, Nov. 2018, doi: 10.1016/j.automatica.2018.07.014.

[37] I. Quanser, "Quanser aero 2 laboratory guide," *Quanser, Tech. Rep.*, Dec. 2022. Available: https://quanserinc.box.com/shared/static/93bfbhxihax1v8bm9at44v56gv01vhee.zip.

[38] W. He, L. Kong, Y. Dong, Y. Yu, C. Yang, and C. Sun, "Fuzzy tracking control for a class of uncertain MIMO nonlinear systems with state constraints," *IEEE Trans. Syst., Man, Cybern. Syst.*, vol. 49, no. 3, pp. 543–554, Mar. 2019, doi: 10.1109/TSMC.2017.2749124.

[39] S. Sui, C. L. P. Chen, and S. Tong, "A novel adaptive NN prescribed performance control for stochastic nonlinear systems," *IEEE Trans. Neural Netw. Learn. Syst.*, vol. 32, no. 7, pp. 3196–3205, Jul. 2021, doi: 10.1109/TNNLS.2020.3010333.

[40] Y. Ren, P. Zhu, Z. Zhao, J. Yang, and T. Zou, "Adaptive fault-tolerant boundary control for a flexible string with unknown dead zone and actuator fault," *IEEE Trans. Cybern.*, vol. 52, no. 7, pp. 7084–7093, Jul. 2022, doi: 10.1109/TCYB.2020.3044144.

[41] L. Zhang and G.-H. Yang, "Observer-based fuzzy adaptive sensor fault compensation for uncertain nonlinear strict-feedback systems," *IEEE Trans. Fuzzy Syst.*, vol. 26, no. 4, pp. 2301–2310, Aug. 2018, doi: 10.1109/TFUZZ.2017.2772879.

Yan Weng received the B.S. degree in robotics engineering and the M.S. degree in control engineering, in 2022 and 2025, respectively, from Guangzhou University, Guangzhou, China, where he is currently working toward the Ph.D. degree in mathematics.

His research interests include adaptive control, reinforcement learning, and robotics.

Zhijia Zhao (Senior Member, IEEE) received the B.Eng. degree in automatic control from the North China University of Water Resources and Electric Power, Zhengzhou, China, in 2010, and the M.Eng. and Ph.D. degrees in automatic control from the South China University of Technology, Guangzhou, China, in 2013 and 2017, respectively.

He is currently a Professor with the School of Mechanical and Electrical Engineering, Guangzhou University, Guangzhou, China. His research interests include adaptive and learning control, flexible mechanical systems, and robotics.

Dr. Zhao has been an Associate Editor of IEEE TRANSACTIONS ON AUTOMATION SCIENCE AND ENGINEERING; IEEE TRANSACTIONS ON NEURAL NETWORKS AND LEARNING SYSTEMS; IEEE TRANSACTIONS ON SYSTEMS, MAN, AND CYBERNETICS: SYSTEMS; and other flagship journals.

Di Zhang received the B.Eng. degree in robotics engineering in 2022 from Guangzhou University, Guangzhou, China, where he is currently working toward the M.Eng. degree in control engineering.

His research interests include adaptive control, intelligent control, and robotics.

Zhijie Liu (Member, IEEE) received B.Sc. degree in electrical engineering and automation from China University of Mining and Technology Beijing, Beijing, China, in 2014, and the Ph.D. degree in control theory and control engineering from Beihang University, Beijing, in 2019.

He was a Research Assistant with the Department of Electrical Engineering, University of Notre Dame, Notre Dame, IN, USA, in 2017. He is currently a Full Professor with the School of Intelligence Science and Technology, University of Science and Technology Beijing, Beijing. His research interests include adaptive control, modeling and vibration control for flexible structures, and distributed parameter system.

Keum-Shik Hong (Life Fellow, IEEE) received the B.S. degree in mechanical design from Seoul National University, Seoul, South Korea, in 1979, the M.S. degree in mechanical engineering from Columbia University, New York, NY, USA, in 1987, and the M.S. degree in applied mathematics and the Ph.D. degree in mechanical engineering from the University of Illinois at Urbana-Champaign, Urbana, IL, USA, in 1991.

He is a Professor with the School of Mechanical Engineering, Pusan National University, South Korea, since 1993. His research interests include brain–computer interface, nonlinear systems theory, adaptive control, and distributed parameter systems. He served as an Associate Editor of *Automatica*, from 2000 to 2006, as an Editor-in-Chief of the *Journal of Mechanical Science and Technology*, from 2008 to 2011, and is serving as the Editor-in-Chief of the *International Journal of Control, Automation, and Systems*.

Dr. Hong was a past President of the Institute of Control, Robotics and Systems (ICROS), Korea, and is the President of the Asian Control Association. He is a fellow of the Korean Academy of Science and Technology, an ICROS Fellow, and a Member of the National Academy of Engineering of Korea. He has received many awards, including the Best Paper Award from the KFSTS of Korea (1999) and the Presidential Award of Korea (2007).